

# Solar Influence on Nuclear Decay Rates: Constraints from the MESSENGER Mission

E. Fischbach<sup>1</sup> • K.J. Chen • R.E. Gold •  
J.O. Goldsten • D.J. Lawrence • R. J. McNutt, Jr.  
• E.A. Rhodes • J.H. Jenkins<sup>2</sup> • J. Longuski

**Abstract** We have analyzed  $^{137}\text{Cs}$  decay data, obtained from a small sample onboard the MESSENGER spacecraft en route to Mercury, with the aim of setting limits on a possible correlation between nuclear decay rates and solar activity. Such a correlation has been suggested recently on the basis of data from  $^{54}\text{Mn}$  decay during the solar flare of 13 December 2006, and by indications of an annual and other periodic variations in the decay rates of  $^{32}\text{Si}$ ,  $^{36}\text{Cl}$ , and  $^{226}\text{Ra}$ . Data from five measurements of the  $^{137}\text{Cs}$  count rate over a period of approximately 5.4 years have been fit to a formula which accounts for the usual exponential decrease in count rate over time, along with the addition of a theoretical solar contribution varying with MESSENGER-Sun separation. The indication of solar influence is then

characterized by a non-zero value of the calculated parameter  $\xi$ , and we find  $\xi = (2.8 \pm 8.1) \times 10^{-3}$  for  $^{137}\text{Cs}$ . A simulation of the increased data that can hypothetically be expected following Mercury orbit insertion on 18 March 2011 suggests that the anticipated improvement in the determination of  $\xi$  could reveal a non-zero value of  $\xi$  if present at a level consistent with other data.

**Keywords** astroparticle physics – nuclear reactions – Sun:particle emission

In a recent series of papers (Jenkins and Fischbach 2009; Jenkins et al. 2009; Fischbach et al. 2009; Sturrock et al. 2010a; Javorsek II et al. 2010; Sturrock et al. 2010b) evidence has been presented for a possible solar influence on nuclear decay rates. Data analyzed by Jenkins and Fischbach (2009) and Fischbach et al. (2009) indicate a possible correlation between the solar flare of 13 December 2006 and a decrease in the measured decay rate of  $^{54}\text{Mn}$  coincident in time with the flare. An analysis of data from Brookhaven National Laboratory (BNL) on the measured decay rates of  $^{32}\text{Si}$  and  $^{36}\text{Cl}$ , and from the Physikalisch-Technische Bundesanstalt (PTB) in Germany on the measured decay rates of  $^{226}\text{Ra}$  and its daughters, show that both data sets exhibit similar annual variations in their respective decay rates (Jenkins et al. 2009; Fischbach et al. 2009). Similar periodic effects have been reported by Parkhomov and Maklyaev (2004); Parkhomov (2005, 2010b,c,d), Ellis (1990), Falkenberg (2001), Baurov et al. (2001, 2007), and citetshn98,shn00, and more recently by Jenkins et al. (Submitted to NIM-A, 2011), in data from The Ohio State University. In addition to annual periodicities, evidence for other periodicities in decay data possibly associated with solar rotation is reported in Sturrock et al. (2010a), Sturrock et al. (2010b), Fischbach et al. (2011), and Sturrock et al. (2011), including evidence for a period of  $\sim 33$  days, and for a 2.11

---

E. Fischbach

Department of Physics, Purdue University, West Lafayette, IN 47907 USA

K.J. Chen

Department of Mathematics, Purdue University, West Lafayette, IN 47907 USA

R.E. Gold

J.O. Goldsten

D.J. Lawrence

R. J. McNutt, Jr.

E.A. Rhodes

Johns Hopkins University Applied Physics Laboratory, Laurel, MD 20723-6099 USA

J.H. Jenkins

School of Nuclear Engineering, Purdue University, West Lafayette, IN 47907 USA

J. Longuski

School of Aeronautical and Astronautical Engineering, Purdue University, West Lafayette, IN 47907 USA

<sup>1</sup>525 Northwestern Ave. West Lafayette, IN 47907 USA, ephraim@purdue.edu

<sup>2</sup>Department of Physics, Purdue University, West Lafayette, IN 47907 USA

$\text{yr}^{-1}$  Rieger-like periodicity. Since none of the rotation-related periodic signals (in what should be randomly distributed data) corresponds to any known terrestrial influence, these results support the inference of a solar origin to time-varying nuclear decay rates, through some as yet unknown mechanism (Fischbach et al. 2011).

The interpretation of the data in Jenkins and Fischbach (2009), Jenkins et al. (2009), and Fischbach et al. (2009) have been questioned by Cooper (2009); Norman et al. (2009); Semkow et al. (2009), however, Jenkins et al. (2010) addressed all of those questions. Nonetheless, the nature of the effects reported in the original references remains uncertain at present, particularly since solar flares are not always correlated in detectable changes in nuclear decay rates (Parkhomov 2010a). However, if nuclear decays can in fact be influenced by the Sun, and specifically by the varying distance between a decaying source and the Sun, then data from the MESSENGER mission to Mercury (Solomon et al. 2007) could lead to significant constraints on the magnitudes of such effects on the examined isotope, given that the MESSENGER-Sun distance has varied from 1.0689 AU to 0.30748 AU. The object of the present paper is to use decay data from a sample of  $^{137}\text{Cs}$  onboard MESSENGER to search for a possible variation of the  $^{137}\text{Cs}$  decay parameter  $\lambda$ , or its half-life  $T_{1/2} = \ln 2 / \lambda = 30.07 \text{ yr}$  (Baum et al. 2002), over the course of the mission to date.

The MESSENGER spacecraft was launched on 3 August 2004, and Mercury orbit insertion (MOI) occurred as scheduled on 18 March 2011. The objective of MESSENGER is to study Mercury from a highly eccentric orbit with a low-altitude periapsis. Following launch, several gravity-assist maneuvers were carried out by the MESSENGER spacecraft. These included a close flyby of the Earth approximately one year after launch (to reduce the required launch energy), and a subsequent deep-space maneuver to put MESSENGER on course for two Venus flybys to further lower the perihelion distance. Three Mercury flybys (with a leveraging deep-space maneuver in between successive Mercury gravity assists) were used to gradually slow the spacecraft with respect to Mercury. (A timeline for the MESSENGER mission trajectory is presented in Figure 1.) Among the seven instruments that comprise the MESSENGER physics payload is a Gamma-Ray and Neutron Spectrometer (GRNS) (Goldsten et al. 2007), whose purpose is to map the elemental composition of the surface of Mercury. Galactic cosmic rays (GCRs) incident on the surface of Mercury produce characteristic gamma-rays and neutrons, which are detected by the GRNS,

from which inferences can be drawn about the planet's surface composition. The Gamma-Ray Spectrometer (GRS) portion of the GRNS is a high-purity germanium (HPGe) sensor surrounded by a plastic scintillator anti-coincidence shield (ACS). During normal operation, the HPGe sensor is cooled to cryogenic temperatures using a miniature mechanical cooler. The mechanical cooler has a limited operational life, with an expected mean time to failure of approximately one year. Because the primary goal of the GRS is to map Mercury's composition for one Earth year, the GRS has been used sparingly during MESSENGER's seven-year cruise phase. The few times the GRS has been turned on have been to verify its operation and to make gamma-ray measurements of Mercury during the three Mercury flybys (Rhodes 2011).

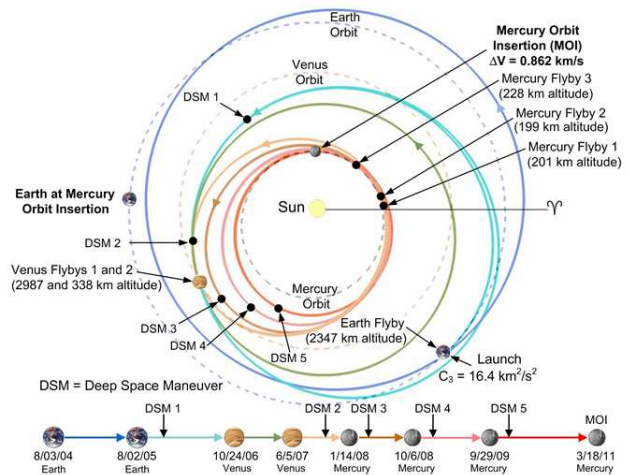


**Fig. 1** Timeline for the MESSENGER mission. Launch from Earth was on 4 March 2004, and Mercury orbit insertion (MOI) occurred on 18 March 2011. During the MESSENGER mission the MESSENGER-Sun distance has varied from 1.0689 A.U. to 0.30748 A.U., a wide enough range to test the hypothesis of a time-varying nuclear decay rate that depends on distance from the Sun. Figure courtesy of NASA/Johns Hopkins University Applied Physics Laboratory/Carnegie Institution of Washington.

Shortly after launch, readings from the GRS while in deep space revealed the presence of an unexpected small  $^{137}\text{Cs}$  source. It is not known if this  $^{137}\text{Cs}$  source is incorporated into the GRS sensor or some part of its housing. Nevertheless, because this source has been onboard MESSENGER from launch, its presence allows us, serendipitously, to set limits on the influence of solar activity on  $^{137}\text{Cs}$  decay. To date, five sets of measurements of the  $^{137}\text{Cs}$  decay rate have been made during periods denoted by Cruise 0 through Cruise 4, and more are expected after MOI. In what follows, we

develop a formalism to study a possible solar influence on  $^{137}\text{Cs}$  decay, and we then apply this formalism to the existing data. We conclude with a discussion of the improvements that can be expected from data to be acquired after MOI.

## 1 Theoretical Formalism

The presence of the  $^{137}\text{Cs}$  source onboard MESSENGER provides an opportunity to test whether the  $^{137}\text{Cs}$  decay rate varies with MESSENGER-Sun distance. Following the discussion presented in Fischbach et al. (2009) we assume that the beta decay rate  $dN(t)/dt \equiv \dot{N}(t)$  of a sample containing  $N(t)$  unstable nuclei can be written in the form

$$\frac{-dN(t)}{dt} = \lambda(t)N(t) = [\lambda_0 + \lambda_1(\vec{r}, t)]N(t), \quad (1)$$

where  $\lambda_0$  represents the intrinsic contribution to the  $\beta$ -decay rate arising from the conventional weak interaction along with a possible time-independent background arising from new interactions. The time-dependent perturbation  $\lambda_1(\vec{r}, t)$  is also a function of the distance  $r = |\vec{r}|$  between the decaying nucleus and the source, here assumed to be the Sun. For a perturbation whose influence on a decaying nucleus varies as  $1/r^n$ , where  $n$  is an integer,  $\lambda_1(\vec{r}, t)$  can be expressed in the form

$$\lambda_1(\vec{r}, t) = \lambda_0 \xi^{(n)} \left[ \frac{R}{r(t)} \right]^n, \quad (2)$$

where  $R \equiv r(t=0)$ , and  $\xi^{(n)}$  is the parameter we are interested in constraining. In what follows we focus initially on  $\xi^{(2)} \equiv \xi$ , which is the most likely variation that we expect, (i.e., an inverse-square law). Results for  $n = 1$  and  $n = 3$ , which are the next most likely alternatives to  $n = 2$ , can be analyzed in a similar way. We note from Eqs. (1) and (2) that  $\xi$  is not a universal constant since it depends on the specified initial values  $R$  and  $t = 0$ . In the present paper we define  $t = 0$  as the launch time, in which case  $R = 1 \text{ AU} = 1.495979 \times 10^8 \text{ km}$ . Integrating Eq. (1) we find

$$N(t) = N_0 \exp\{-\lambda_0[t + \xi I(t)]\}, \quad (3)$$

$$-\frac{dN(t)}{dt} = \lambda_0 N_0 \exp(-\lambda_0 t) \left\{ 1 + \xi \left[ \frac{R^2}{r^2(t)} - \lambda_0 I(t) \right] \right\}, \quad (4)$$

$$I(t) = \int_0^t dt' \left[ \frac{R}{r(t')} \right]^2. \quad (5)$$

We note from Eqs. (3-5) that since  $I(0) = 0$ , the effective  $^{137}\text{Cs}$  decay constant at  $t = 0$  is  $\lambda \equiv \lambda_0(1 + \xi)$ , where  $\lambda = 6.311(19) \times 10^{-5} \text{ d}^{-1}$  is the standard value measured on Earth (at 1 AU) corresponding to  $T_{1/2} = 30.07(9) \text{ yr}$ . It is convenient to rewrite Eq. (4) in terms of directly measured quantities by first expressing  $\lambda_0$  in terms of  $\lambda$ , and then eliminating the unknown  $N_0$  by taking appropriate ratios. To lowest order in  $\xi \ll 1$  we find

$$\begin{aligned} e^{+\lambda t} \frac{dN(t)/dt}{dN(t=0)/dt} &\cong 1 + \xi \left[ \frac{R^2}{r^2(t)} - \lambda I(t) + \lambda t - 1 \right] \\ &\equiv 1 + \xi B(t). \end{aligned} \quad (6)$$

We note from Eq. (6) that since  $B(t=0) = 0$  the count rate ratio approaches unity as  $t \rightarrow 0$ , as expected. Comparing Eqs. (4) and (6), the additional terms in the square brackets in Eq. (6) arise from computing the indicated ratio, and then expressing the final result in terms of the laboratory value  $\lambda$ .

In principle, the left hand side of Eq. (6) and  $B(t)$  are directly measurable, and hence can be used to set limits on  $\xi$ . These limits can then be compared to those obtained in the laboratory. In practice, however,  $dN(t=0)/dt$  was not measured, and hence our limits on  $\xi$  were determined from ratios of count rates obtained from measurements made during the five cruise periods. A summary of the data obtained from these measurements is presented in Table 1. Among the entries in this table, the precision of the data which enter into the calculation of  $B(t)$  is such that the errors on  $B(t)$  can be neglected compared to those arising from the count rates (see discussion below). The integral  $I(t)$ , which is exhibited in Figure 2, accounts for the cumulative  $\xi$ -dependent contributions to the  $^{137}\text{Cs}$  decay rate arising from both the change in MESSENGER-Sun distance, as well as from the normalization relation  $\lambda = \lambda_0(1 + \xi)$ .

Returning to Eq. (6), the experimentally interesting quantities are the ratios

$$\frac{[\exp(\lambda t_i) dN(t_i)/dt]}{[\exp(\lambda t_0) dN(t_0)/dt]},$$

where  $t_0$  and  $t_i$  ( $i = 1, 2, 3, 4$ ) denote the start times of the five cruise measurement periods. These five measurements thus determine four ratios which, along with the corresponding values of  $B(t_i)$ , can be used to obtain  $\xi$ .

## 2 Analysis of the $^{137}\text{Cs}$ Count Rates

The MESSENGER GRS data analyzed in this paper are made publicly available in the NASA Planetary

**Table 1** Summary of  $^{137}\text{Cs}$  decay data from the MESSENGER mission. For each of the five measurement periods ( $t_0, t_1, t_2, t_3, t_4$ ), these data include the calculated values of  $I(t)$ ,  $B(t)$ , and  $\Delta(t)$ , for a perturbation varying as  $1/r^2$

	Cruise 0	Cruise 1	Cruise 2	Cruise 3	Cruise 4
	Initial checkout	Mercury Flyby 1	Mercury Flyby 2	Mercury Flyby 3	Final checkout
Calendar date	16 Nov 2004	14 Jan 2008	6 Oct 2008	2 Oct 2009	14 Apr 2010
Julian date	2453322.500	2454478.500	2454744.500	2455102.500	2455300.500
Distance from the Sun (km)	160599579.0277	54595403.8012	52751315.2631	48132083.3548	63523375.7902
Elapsed time since Cruise 0 (days)	0.0	1156.0	1422.0	1780.0	1978.0
Mean count rate in peak (cps)	$0.100 \pm 0.0012$	$0.0942 \pm 0.0019$	$0.0933 \pm 0.0020$	$0.0886 \pm 0.0017$	$0.0886 \pm 0.0020$
Total accumulation time (hours)	60.00	45.00	40.00	60.00	39.00
$I(t)$ (days)	91.173	2284.190	3408.077	5162.823	6228.370
$B(t)$	-0.1316	6.4397	6.9235	8.4530	4.2842
$\Delta(t)$	0.0000	6.5751	7.0551	8.5847	4.4159

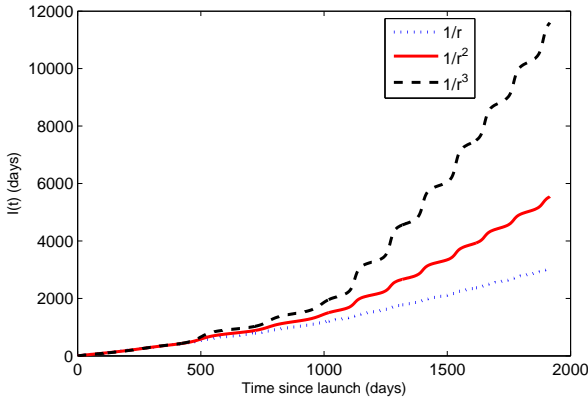


**Fig. 2** Plots of the integrals  $I(t)$ , for  $n = 1, 2, 3$ , in Eq. (2). The integrals are defined in analogy to  $I^{(2)}(t)$  in Eq. (5).

Data System (PDS) archive<sup>1</sup> according to the schedule given at the PDS web site. Table 1 lists the time periods for each of the five cruise measurements. Each of the data collection periods lasted for greater than 24 hours, and some for over 60 hours. To ensure that the data analyzed here were acquired when the instrument parameters and background were reasonably constant, appropriate time windows were selected within each data collection period. For example, the Cruise 0 period took place during the declining phase of a solar particle event, so the background was relatively high during the early portion of this collection period. Thus, the selected time window for the Cruise 0 period was the last 60 hours of the collection period, when the background was the lowest. For the other data collection periods, data were excluded during the Mercury flybys and when instrument parameters were varied for sensor testing.

Figure 3 shows an example anticoincidence pulse-height spectrum from the Cruise 0 data collection pe-

riod. Figure 3a shows the electronic pulser peak used to correct for detector dead time; Figure 3b shows the 662 keV peak from the  $^{137}\text{Cs}$  decay. GRS dead time is largely driven by a 1000 Hz raw counting rate in the ACS. The dead time is monitored by a 7.62939 Hz electronic pulse fed directly across the HPGGe detector. The pulser line appears at a high energy in the pulse-height spectrum, far away from other prominent gamma-ray lines. The total counts in the pulser peak are obtained by fitting a linear function to the underlying background, subtracting this background from the pulse height spectra, and summing the net counts. The live time fraction is the ratio of the measured counts to the expected number of pulser counts. For the five measurement periods, the live time fraction varied from 0.9 to 0.94.

The total counts in the  $^{137}\text{Cs}$  peak are determined by dividing the spectra by the live time fraction, fitting a second-degree polynomial function to the background above and below the peak (dashed line in Figure 3b), subtracting this background, and then summing the net counts (dot-dashed line) within a window around the peak. The count rate uncertainties are calculated by assuming all uncertainties are due to Poisson counting statistics. Specifically, if the total net counts within the energy window are  $N_{Net} = N_{Spec} - N_{Back}$ , where  $N_{Spec}$  and  $N_{Back}$  are the total spectrum and background counts within the energy window, respectively, then the total count uncertainty,  $\sigma_{Net}$ , is

$$\sigma_{Net} = \sqrt{\sigma_{Spec}^2 + \sigma_{Back}^2} = \sqrt{N_{Spec} + N_{Back}}. \quad (7)$$

The corresponding count rate uncertainty is:

$$\sigma_{dN/dt} = \left( \frac{dN}{dt} \right) \frac{\sigma_{Net}}{N_{Net}}. \quad (8)$$

The uncertainty associated with the live time correction is neglected because its magnitude is almost an order

<sup>1</sup>(<http://geo.pds.nasa.gov/missions/messenger/index.htm>)

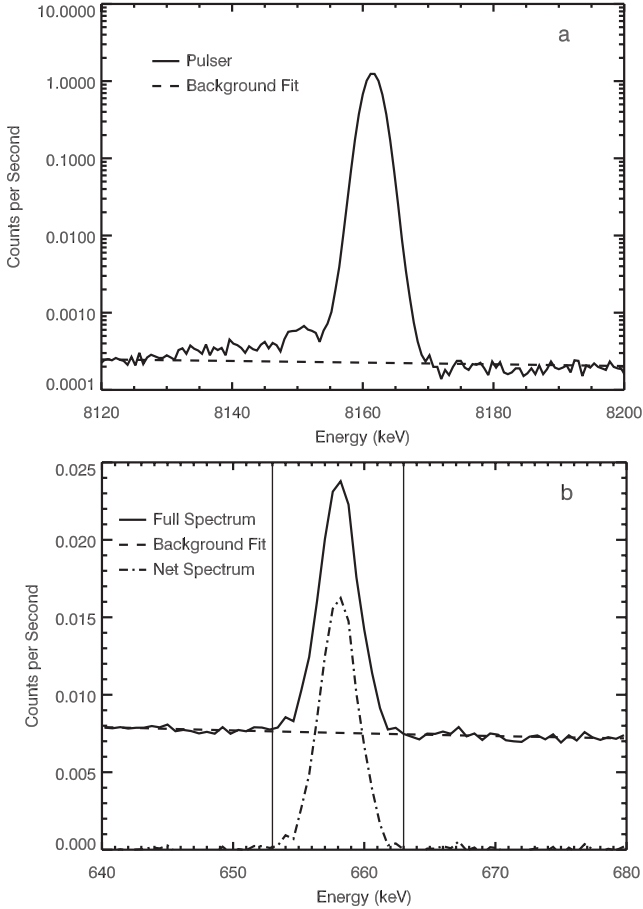


**Fig. 3** Measured GRS pulse height spectra taken during the Cruise 0 data collection period. (a) Pulsar data (solid line) and background (dashed line) fit to the pulser data; (b)  $^{137}\text{Cs}$  data (solid line), background in the region around the  $^{137}\text{Cs}$  line (dashed line), and net  $^{137}\text{Cs}$  spectrum (dot-dashed line). Solid vertical lines show the energy window over which the counts are determined.

of magnitude lower than that of the uncertainty for the  $^{137}\text{Cs}$  peak.

One other point regarding the GRS is that in order to reduce energy spreading effects from GCR radiation damage, the GRS is periodically annealed at high temperatures. Since launch, the GRS has been annealed four times (no annealing was carried out prior to Cruise 4). One consequence of annealing is that the active volume of the germanium crystal may shrink slightly, which in turn will slightly reduce the overall detector efficiency. By monitoring the position of the pulser peak after each annealing operation, we can estimate the change in detector capacitance, and therefore the active detector volume, by assuming a simple coaxial geometry for the HPGe detector. Since launch, the pulser peak has shifted  $\sim 7\%$ , which equates to less than  $\sim 0.7\%$  loss in detector volume; however, the actual change in detector efficiency at 662 keV is not

easily calculated (perhaps it could be better modeled through a Monte Carlo simulation), but would likely lie between the estimates for the capacitance and volume. Such efficiency changes have not been included in this analysis. For future analyses, efficiency corrections can be monitored and/or included by observing changes in peak counts associated in time with annealing events, as well as by modelling the GRS efficiency response.

### 3 Results

Following the preceding discussion, we have determined  $\xi$  by using Eq. (6) to write

$$e^{\lambda(t_i - t_0)} \frac{[dN(t_i)/dt]}{[dN(t_0)/dt]} \equiv \xi \Delta(t_i) + 1, \quad (9)$$

where  $i = 1, 2, 3, 4$  and  $\Delta(t_i) = B(t_i) - B(t_0) = B(t_i) + 0.1316$ . The starting dates  $t_i$  for Cruise 1, ... Cruise 4, are given in Table 1, as are the calculated values for the integrals  $I(t_i)$  in Eq. (5), and  $\Delta(t_i)$  in Eq. (9). Combining these results with the four ratios obtained from the measured countrates allows us to fit Eq. (9) to a straight line,  $y_i = \xi x_i + b$ , whose slope is  $\xi$ . We find,

$$\xi \equiv \xi^{(2)} = (2.8 \pm 8.1) \times 10^{-3}; \quad b^{(2)} = 1.02 \pm 0.03 \quad (10)$$

The result for  $\xi$  in Eq. (10) can be compared to the annual variation in the  $^{32}\text{Si}/^{36}\text{Cl}$  count rate ratio reported by Jenkins and Fischbach (2009) from their analysis of the data of Alburger et al. (1986) taken at BNL. Jenkins and Fischbach (2009) found a fractional change of  $\sim 3 \times 10^{-3}$  in  $\dot{N}(^{32}\text{Si})/\dot{N}(^{36}\text{Cl})$  from perihelion to aphelion, and this level of sensitivity may be achievable following MOI given the result in Eq. (10) as we now discuss.

### 4 Post-MOI Simulation

The result in Eq. (10) suggests that the availability of a much larger data set following MOI on 18 March 2011 could lead to significantly improved constraints on  $\xi$  for  $^{137}\text{Cs}$ . In this section, we simulate post-MOI data that can be expected in order to estimate the level of improvement on  $\xi$  that might be realized.

We can estimate the post-MOI countrates by re-expressing Eq. (6) and (9) in the form

$$e^{\lambda \Delta t} \left[ \frac{dN(t_i)/dt}{dN(t_1)/dt} \right] \cong 1 + \xi \left[ \frac{R^2}{r^2(t_i)} - \lambda \int_{t_1}^{t_i} dt' \left[ \frac{R}{r(t')} \right]^2 + \lambda \Delta t - 1 - D \right], \quad (11)$$

where

$$D = \frac{R^2}{r^2(t_1)} - \lambda \int_0^{t_1} dt' \left[ \frac{R}{r(t')} \right]^2 + \lambda t_1 - 1 = 9.1542, \quad (12)$$

accounts for the accumulated change in the  $^{137}\text{Cs}$  count rate between Earth launch at  $t = 0$  and MOI at  $t = t_1$ . In Eq. (11),  $t_i$  is the time of the  $i^{\text{th}}$  measurement,  $\Delta t = t_i - t_1$  in days since MOI, and we have used for  $r(t)$  the actual (planned) trajectory ephemeris, calculated by the Jet Propulsion Laboratory HORIZONS system. The simulation was run for slightly more than one Earth-year following MOI, during which each measurement was assumed to last for 11 days. We have also assumed that  $\xi = -0.0031$ , which is compatible with the data of Alburger et al. (1986), and have fixed the initial  $^{137}\text{Cs}$  count rate to be 0.08 cps, which is suggested by the data in Table 1. Under these assumptions, the standard fractional statistical error in each 11-day run is approximately  $\Delta \dot{N}_i / \dot{N}_i = 0.0036$ , and hence the fractional error in the ratio given in Eq. (11) is approximately  $\sqrt{2}(0.0036) = 0.0051$ . A uniformly distributed random error was then added to each expected measurement to simulate uncertainties in the observations. The objective of the simulation is to recover the input value  $\xi = -0.0031$ , and to then determine its associated uncertainty.

The results of our simulation are shown in Figs. 4 and 5. In Fig. 4, the error bars represent the  $1/\sqrt{N}$  errors in each point, and the asterisks (\*) denote the result of a random measurement of the count rate ratio within the  $1/\sqrt{N}$  range. The solid line represents the expected results in the null-case ( $\xi = 0$ ), corresponding to a pure exponential decay in time. Fitting the simulated data to Eq. (11), we find (see Fig. 5),

$$\xi = (-3.1 \pm 0.4) \times 10^{-3}, \quad (13)$$

for the post-MOI data that we have generated. We note from Eq. (13) that the central value of  $\xi$  is in agreement with the input value  $\xi = -0.0031$  that we have used. More significantly, the uncertainty in  $\xi$  is sufficiently small to suggest that a non-zero value of  $\xi$  near the nominal level that we have assumed might be detectable using a more sophisticated analysis of the actual post-MOI MESSENGER data.

## Acknowledgements

The work of EF is supported in part by U.S. DOE contract No. DE-AC02-76ER071428.

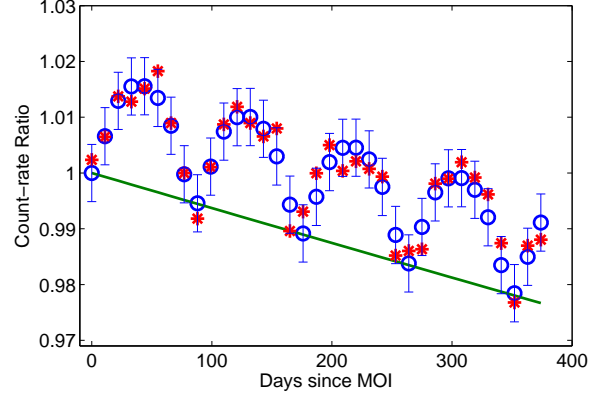


**Fig. 4** Simulated count rates as a function of time. The error bars represent the  $1/\sqrt{N}$  statistical uncertainties at each point, and the asterisks (\*) are the results of simulated “observations”. The solid line is the prediction for  $\xi = 0$ , corresponding to a pure exponential decay in time.

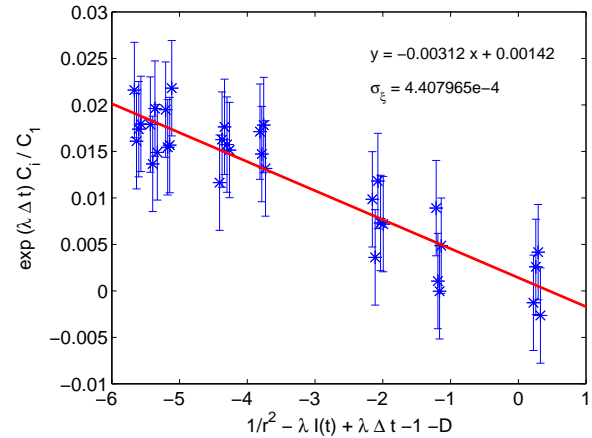


**Fig. 5** Determination of  $\xi$  from the simulated data. The vertical and horizontal axes correspond, respectively, to the left-hand and right-hand sides of Eq. (11), where  $C_i \equiv \dot{N}_i$ , etc., and the solid line gives the best fit to the simulated data. The inferred value of  $\xi$  is given in Eq. (13).



## References

- Alburger, D.E., Harbottle, G., Norton, E.F.: *Earth and Planetary Science Letters* **78**(2-3), 168 (1986)
- Baum, E.M., Knox, H.D., Miller, T.R.: *Nuclides and Isotopes: Chart of the Nuclides*, 16th edn. Lockheed Martin (KAPL), (2002)
- Baurov, Y.A., Konradov, A.A., Kushniruk, V.F., Kuznetsov, E.A., Sobolev, Y.G., Ryabov, Y.V., Senkevich, A.P., Zadorozsny, S.V.: *Modern Physics Letters A* **16**(32), 2089 (2001)
- Baurov, Y.A., Sobolev, Y.G., Ryabov, Y.V., Kushniruk, V.F.: *Physics of Atomic Nuclei* **70**(11), 1825 (2007)
- Cooper, P.S.: *Astroparticle Physics* **31**(4), 267 (2009)
- Ellis, K.J.: *Physics in Medicine and Biology* **35**(8), 1079 (1990)
- Falkenberg, E.D.: *Apeiron* **8**(2), 14 (2001)
- Fischbach, E., Jenkins, J.H., Sturrock, P.A.: *arXiv* (arXiv:1106.1470v1 [nucl-ex]), 1 (2011)
- Fischbach, E., Buncher, J., Gruenwald, J., Jenkins, J., Krause, D., Mattes, J., Newport, J.: *Space Science Reviews* **145**(3), 285 (2009)
- Fischbach, E., Sturrock, P.A., Jenkins, J.H., Javorsek II, D., Buncher, J.B., Gruenwald, J.T.: In: Kostelecky, V.A. (ed.) *Proceedings of the Fifth Meeting on CPT and Lorentz Symmetry*, p. 168. World Scientific: Singapore, (2011)
- Goldsten, J., Rhodes, E., Boynton, W., Feldman, W., Lawrence, D., Trombka, J., Smith, D., Evans, L., White, J., Madden, N., Berg, P., Murphy, G., Gurnee, R., Strohehn, K., Williams, B., Schaefer, E., Monaco, C., Cork, C., Del Eckels, J., Miller, W., Burks, M., Hagler, L., DeTeresa, S., Witte, M.: *Space Science Reviews* **131**(1), 339 (2007)
- Javorsek II, D., Sturrock, P.A., Lasenby, R.N., Lasenby, A.N., Buncher, J.B., Fischbach, E., Gruenwald, J.T., Hoft, A.W., Horan, T.J., Jenkins, J.H., Kerford, J.L., Lee, R.H., Longman, A., Mattes, J.J., Morreale, B.L., Morris, D.B., Mudry, R.N., Newport, J.R., O'Keefe, D., Petrelli, M.A., Silver, M.A., Stewart, C.A., Terry, B.: *Astroparticle Physics* **34**(3), 173 (2010)
- Jenkins, J.H., Fischbach, E.: *Astroparticle Physics* **31**(6), 407 (2009)
- Jenkins, J.H., Mundy, D.W., Fischbach, E.: *Nuclear Instruments and Methods in Physics Research Section A: Accelerators, Spectrometers, Detectors and Associated Equipment* **620**(2-3), 332 (2010)
- Jenkins, J.H., Fischbach, E., Buncher, J.B., Gruenwald, J.T., Krause, D.E., Mattes, J.J.: *Astroparticle Physics* **32**(1), 42 (2009)
- Jenkins, J.H., Herminghuysen, K.R., Blue, T.E., Fischbach, E., Javorsek II, D., Kauffman, A.C., Mundy, D.W., Sturrock, P.A., Talnagi, J.A.: *Additional experimental evidence for a solar influence on nuclear decay rates* (Submitted to NIM-A, 2011)
- Norman, E.B., Browne, E., Shugart, H.A., Joshi, T.H., Firestone, R.B.: *Astroparticle Physics* **31**(2), 135 (2009)
- Parkhomov, A.G.: *International Journal of Pure and Applied Physics* **1**(2), 119 (2005)
- Parkhomov, A.G.: *ArXiv* (arXiv:1006.2295v1 [physics.gen-ph]), 1 (2010a)
- Parkhomov, A.G.: *ArXiv* (arXiv:1010.1591v1 [physics.gen-ph]) (2010b)
- Parkhomov, A.G.: *ArXiv* (arXiv:1012.4174v1 [physics.gen-ph]) (2010c)
- Parkhomov, A.G.: *ArXiv* (arXiv:1004.1761v1 [physics.gen-ph]) (2010d)
- Parkhomov, A.G., Maklyaev, E.F.: *Fizicheskaya Mysl Rossii* (1), 1 (2004)
- Rhodes, E.A.: *In preparation* (2011)
- Semkow, T.M., Haines, D.K., Beach, S.E., Kilpatrick, B.J., Khan, A.J., O'Brien, K.: *Physics Letters B* **675**(5), 415 (2009)
- Solomon, S., McNutt, R., Gold, R., Domingue, D.: *Space Science Reviews* **131**(1), 3 (2007)
- Sturrock, P.A., Buncher, J.B., Fischbach, E., Gruenwald, J.T., Javorsek II, D., Jenkins, J.H., Lee, R.H., Mattes, J.J., Newport, J.R.: *Astroparticle Physics* **34**(2), 121 (2010a)
- Sturrock, P.A., Fischbach, E., Jenkins, J.H.: *Solar Physics* DOI: 10.1007/s11207-011-9807-5 (2011)
- Sturrock, P.A., Buncher, J.B., Fischbach, E., Gruenwald, J.T., Javorsek II, D., Jenkins, J.H., Lee, R.H., Mattes, J.J., Newport, J.R.: *Solar Physics* **267**(2), 251 (2010b)